Journal of Computers Vol. 36 No. 1, February 2025, pp. 255-270
https://doi.org/10.63367/199115992025023601017

Optimization Simulation Analysis of Noise Reduction Based on the Mechanism of Noise Generation and Transmission in Turbine Compressors

Han Gao[1], Hao Wang[2], Ming-Rui Zhang[3],
Xiao-Lu Ma[4*], and Yang-Yang Yu[1]

[1] School of Mechanical Engineering, Tianjin Renai College,
Tianjin 301636, China
gaohantianjin@163.com, yuyangyang@tju.edu.cn

[2] Tianjin Hongyuan Machinery Technology Co., Ltd,
Tianjin 300190, China
wangyi891210@163.com

[3] Tianjin Tiankan Lantai Engineering Technology Consulting Co., Ltd,
Tianjin 301812, China
17848009526@163.com

[4] Tianjin Renai College Employment Guidance Service Center,
Tianjin 301636, China
136761142@qq.com

Received 24 January 2025; Revised 1 February 2025; Accepted 11 February 2025

Abstract. Turbine compressors are highly efficient power compressors widely used in fields such as chemical engineering and refrigeration. However, there is vibration during compressor operation, and the vibration noise is amplified through the transmission path of the compressor structure itself, which has adverse effects on the production environment and the health of operators. Therefore, this article analyzes the mechanism of vibration noise generation and vibration propagation in turbine compressors, and constructs a vibration and vibration transmission path model. Based on the above two models, by collecting and separating sound, the generation of vibration at the source can be reduced. At the same time, improving the vibration transmission path can effectively reduce the transmission of vibration noise in turbine compressors. Then, by studying the sound radiation characteristics of the compressor housing, it helps to reduce the vibration of the compressor. The path of noise propagation, Finally, by constructing sound radiation characteristics and modal analysis characteristics, the outer shell of the turbine compressor is optimized to determine the reasonable distribution positions of reinforcement ribs and rib plates, thereby reducing shell vibration and radiation noise.

Keywords: vibration mechanism, transmission path, sound radiation characteristics, modal simulation

1 Introduction

Turbine compressors as an efficient and reliable power compressor, it is widely used in various industrial fields. Its core lies in the interaction force between the high-speed rotating impeller and the airflow, which increases the gas pressure and converts the kinetic energy of the airflow into pressure energy, thereby achieving gas compression and transportation. Turbine compressors are mainly divided into two categories: axial flow and centrifugal flow, which are suitable for different process requirements depending on the direction of gas flow. Turbine compressors play an irreplaceable role in many important sectors such as petroleum, chemical, natural gas transportation, metallurgy, refrigeration, and mine ventilation [1]. For example, in the petrochemical industry, turbine compressors are used to increase the pressure of feed gas to meet the requirements of subsequent processes; During natural gas transportation, turbine compressors are used for pressurization to ensure that natural gas can be

* Corresponding Author

transported over long distances and efficiently to its destination. In addition, turbine compressors are commonly used in air separation equipment to provide a stable high-pressure gas source for processes such as oxygen and nitrogen production [2].

Although turbine compressors have wide application value in industrial production, the vibration problems that exist during their operation cannot be ignored. The vibration of turbine compressors not only reduces the operating efficiency and service life of the equipment, but may also have adverse effects on the production environment and personnel health. Specifically, the vibration problem of turbine compressors is mainly manifested in the following aspects:

1) Unbalanced rotor: During high-speed rotation, the rotor of a turbine compressor may experience vibration due to uneven material density and machining errors. This vibration will intensify with the increase of speed, posing a threat to the stable operation of the equipment.

2) Coupling misalignment: The rotors of turbine compressors are usually connected through couplings. If the coupling is misaligned during installation or operation, it will cause additional vibration and noise. Under long-term operation, this misalignment may also lead to serious consequences such as bearing damage and seal failure.

3) Bearing failure: Bearings are critical components in turbine compressors that bear loads and support rotors. If the bearing selection is improper, the installation accuracy is insufficient, or the lubrication is poor, it may lead to bearing failure, which in turn can cause vibration. Oil film vortex and oil film oscillation are common vibration forms in bearing failures, which have a significant impact on the life of the rotor and shaft.

4) Surge phenomenon: Surge is an unstable phenomenon that may occur during the operation of turbine compressors. When there are periodic low-frequency and large amplitude fluctuations in the flow rate and pressure of gas in the compressor and pipeline, surge occurs. Surge not only causes strong vibration of the unit, but may also cause damage to the equipment [3].

Given the importance of turbine compressors in industrial production and their vibration issues, this article aims to explore methods and techniques for reducing the vibration noise of turbine compressors. Through in-depth analysis of the causes and mechanisms of vibration in turbine compressors, combined with modern control theory and engineering techniques, effective vibration control strategies are proposed. The specific research content includes:

1) In depth analysis of turbine compressors was conducted, and the analysis and modeling of the vibration mechanism and transmission path of turbine compressors were completed

2) Completed the analysis of the acoustic radiation characteristics of the compressor casing, constructed acoustic radiation characteristics and modal analysis models, optimized the turbine compressor casing, determined the reasonable distribution positions of reinforcement ribs and rib plates, and constructed a sound analysis model.

3) Perform modal analysis, transient dynamics simulation, and acoustic radiation simulation on the optimized model with the same boundary conditions, and compare the optimization effect of surface acoustic radiation noise reduction through the results of pre - and post simulation.

2 Related Work

In terms of reducing compressor vibration noise, many scholars have conducted relevant research. From a structural perspective, turbine compressors first belong to rotating machinery and therefore possess all the characteristics of rotating machinery in vibration, as well as the characteristics of compressors. Therefore, the research results on noise localization and noise reduction methods in rotating and compression equipment can serve as a research basis.

Wenzhuo Zhang from Dalian University studied the noise characteristics of variable frequency scroll compressors under different operating conditions and speeds to address the issue of excessive noise. Then, in a fully anechoic chamber, a noise acquisition system was used to test the noise characteristics of the compressor under different operating conditions and speeds. It was found that the scroll compressor operates at a medium speed (70) There is additional noise below, which mainly comes from the exhaust valve mechanism. Based on this, the exhaust valve mechanism is optimized by using a disc exhaust valve instead of a reed valve to reduce the additional noise caused by the valve seat hitting in the opposite direction. After improvement, the total sound pressure level of the compressor decreases by 0.99, 3.83, 1.82 dB at medium temperature conditions and speeds of 30, 70, 110 r/s, respectively, while the decrease is more significant at low temperature conditions. The total sound pressure level decreases by 1.42, 4.15, 1.98 at speeds of 30, 70, 110, respectively [4].

Hao Liu analyzed the noise mechanism of the compressor's air valve, considered the characteristics of the suction and exhaust valve group, and constructed the structural domain dynamics equation of the suction and exhaust valve group based on structural dynamics; Establish the fluid control equation for the intake and exhaust valve group using the basic theory of computational fluid dynamics; Establish an acoustic model of the intake and exhaust valve group using Lighthill acoustic analogy method. Considering the physical quantity transfer relationship between the structural fluid acoustic coupling surfaces of the suction and exhaust valve group, a linear compressor suction and exhaust group simulation model based on the structural fluid acoustic coupling is constructed using the ANSYS Workbench multi physics simulation platform to study the aerodynamic noise of the suction and exhaust valve group at different operating frequencies [5].

Shengxi Luo from Chongqing Jiaotong University studied the vibration characteristics of the exhaust valve plate of a rotary vane compressor. By obtaining the relationship between exhaust conditions, geometric parameters, and valve plate vibration displacement, an improved structure of the lift limiter was obtained. Then, a fluid structure coupling model of the improved valve plate exhaust structure was established. Finally, based on the turbulence parameters of the flow field, a wideband noise model of the exhaust valve plate was established to study the distribution law of the improved valve plate noise. With the help of a rotary vane compressor noise test bench, experimental analysis was conducted. After improvement, the noise reduction in the frequency domain of the compressor was significantly reduced, and the noise amplitude at the rear field point was reduced by up to 6% [6].

Bingxiang Long, the research results show that selecting a reasonable ratio of the number of moving and stationary blades of the compressor can effectively suppress the transmission of single tone noise corresponding to the first order BPF of the compressor to the upstream and downstream, but cannot completely eliminate the single tone noise corresponding to the first order BPF. Therefore, the test results after removing the four support plates on the upper half of the compressor inlet casing show that the periodic non-uniform flow field at the compressor inlet induces the vibration of the first stage high aspect ratio moving blades, which is the main cause of abnormal single tone noise and provides direction for the search of vibration sources [7].

Yaozu Li from Qingdao University used near-field measurement, combined with sound pressure, sound array imaging, and sound intensity measurement methods, to determine the noise pressure level, sound intensity level size, frequency spectrum characteristics, and main noise radiation locations of a centrifugal air booster compressor with two ends, four stages, and four stages of cooling in a certain oxygen production plant. Then, the method of using a soundproof cover can achieve a total noise reduction of 29.5dB (A) [8].

Zhongfu Luo from Guizhou University addressed the issue of excessive noise in small double cylinder reciprocating compressors used in oxygen concentrators through Fluent pneumatic simulation and LMS Virtual The Lab multi-body dynamics simulation module is used for joint simulation to solve the pressure pulsation and bearing excitation of the compressor. Based on the structural free mode, pressure pulsation and bearing excitation are added as boundary conditions, and combined with the theory of acoustic vibration coupling, the discrete noise distribution and sound pressure level cloud map of the dual cylinder compressor are obtained. The research results indicate that the peak frequencies that determine the noise level of the compressor are 800, 2500, and 3100 Hz, which are similar to the solid mode frequency; By changing the structural stiffness, the peak noise of the compressor can be reduced. The research results can provide reference for noise control of small reciprocating compressors [9].

Weinan Jin proposed a scheme to install noise reduction structures on the wall of the pipeline downstream of the compressor outlet in order to improve the airflow quality inside the axial compressor and reduce the noise generated during on-site operation. Based on the noise characteristics of axial compressors, a double-layer perforated plate was designed using the perforated plate sound absorption theory proposed by Professor Ma Dayou, while considering the effects of tangential flow and high sound intensity. The sound absorption performance of the sample was tested using the flow tube method. Finally, noise measurements were taken on the upstream and downstream sections of the noise reduction structure during the on-site operation of the compressor. The results show that the perforated plate with noise reduction structure has good sound absorption performance within the designed frequency range, and the noise in the downstream section is significantly reduced [10].

The noise of turbine compressors mainly comes from the vibration generated by the compressor itself during normal operation, and should also include the noise generated by the vibration at the equipment failure point. The vibration of multiple vibration sources is combined to form the overall noise of the compressor during operation. The focus of this study is on the noise reduction of the compressor under normal operating conditions, so the noise problem of the compressor under fault conditions is not considered. Based on the research results of relevant scholars, the structure of this article is as follows:

Chapter 2 introduces the relevant research results, which help to complete the overall design of this article. Chapter 3 completes the construction of the vibration mechanism and vibration transmission path model, and establishes the theoretical analysis basis. Chapter 4 is the optimization analysis process of the vibration generation mechanism and transmission path, and proposes optimization solutions. Chapter 5 is the simulation part, which completes the construction of the simulation model, compares and analyzes the vibration signals of the compressor before and after optimization, and verifies the effectiveness of the method proposed in this article.

3 Analysis and Modeling of Vibration Mechanism and Vibration Transmission Path

As a typical rotary machinery, the various components of a turbine compressor have complex mutual movements. The compressor experiences obvious structural component impacts and friction during startup, acceleration, and shutdown, resulting in vibration and strong radiation noise. The vibration is transmitted along the contact path of the structure, causing vibration of other components. Therefore, this chapter studies the essence of vibration from the perspectives of vibration mechanism and transmission mechanism.

3.1 Compressor Structure

In order to construct an accurate vibration source model of the compressor, the first step is to analyze the structure of the target turbine compressor, which is shown in Fig. 1.

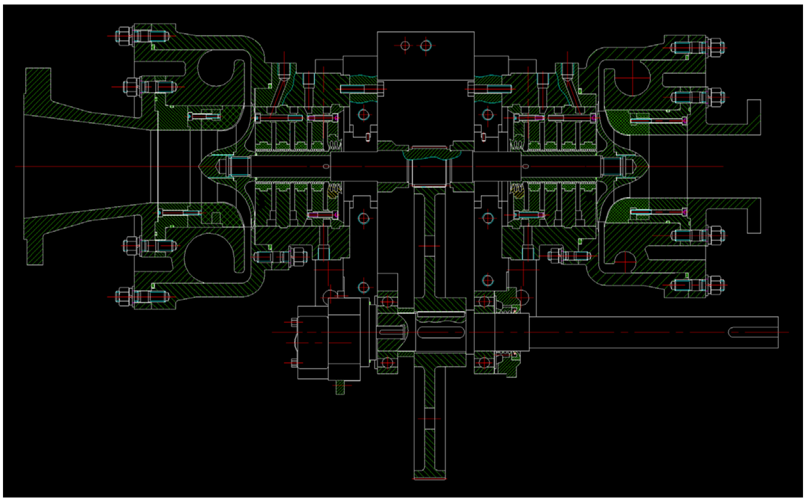

Fig. 1. Schematic diagram of foundation structure of turbine compressor

A typical compressor consists of two parts: the main engine and the auxiliary engine. The main engine includes four parts: compressor, motor, coupling, and housing. The auxiliary engine includes auxiliary systems such as protective gas system, lubrication system, and electrical instrument control system. The unit is built-in, which means that the motor and compressor are connected and placed together in a high-pressure container to operate in high-pressure gas. The compressor is a multi-stage centrifugal compressor, mainly composed of rotor, partition, sealing ring, balance plate, intermediate connecting cylinder, tension cylinder, outlet support body, radial bearing, thrust bearing, outlet horn and other components. The rotor consists of impeller, fixed distance shaft sleeve, floating balance plate, stop pull plate and main shaft. The impeller is slide fitted on the main shaft, and the fixed distance shaft sleeve is axially fixed. The compressor rotor is directly connected to the motor rotor through a coupling to transmit torque. The motor operates at a fixed speed, and the effective operating point of the compressor is changed by changing the number of impeller stages. The compressor and motor rotor are supported by rolling bearings, and the lubrication system supplies lubricating oil to the four rolling bearings [11].

3.2 Modeling of Compressor Working Mechanism

After the compressor is started, the working medium inside, namely air, is in a low or high pressure state, so the gas medium on both sides will exert dynamic gas force on the compressor blades. Assuming that any one of the blades is subjected to a gas force of Fgas , with the point of action being the center position of the blade extending out of the blade groove, pointing towards the low-pressure chamber side [12], the gas force can be expressed as follows:

$$F_{gas} = P_{high} - P_{low} \tag{1}$$

In the formula, P_{high} represents the pressure on the high-pressure side of the blade, and P_{low} represents the pressure on the low-pressure side of the blade. After the compressor is started, the fluid on the left side of the blade undergoes a suction process, and the volume of the medium does not change. The pressure remains at P_{cont} . Before the fluid on the right side of the blade reaches its maximum velocity, the suction process also occurs, and both sides of the blade are equal to the suction pressure, so the gas force is 0. Before the fluid on the left side of the blade reaches its maximum velocity, it is still in the process of suction, and the fluid chamber pressure remains constant at P_{cont} . The fluid on the right side of the blade has gradually decreased from the maximum flow velocity and started the compression process. The gas pressure in the fluid chamber increases accordingly, so the gas force acting on the blade will gradually increase, with a peak gas force of 321 N . When the gas pressure in the fluid chamber on the right side of the blade reaches the exhaust pressure P_{ex} , the gas pressure is maintained at the exhaust pressure value, while the fluid on the left side of the blade gradually decreases in flow velocity and increases in fluid chamber pressure [13]. At this time, the gas force acting on the blade gradually decreases until it drops to 0. The variation law of the force inside the fluid cavity is shown in Fig. 2.

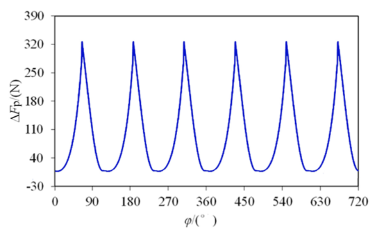

Fig. 2. Schematic diagram of the variation law of the force inside the fluid cavity

When this type of compressor is in operation, the rotor drives the blades to rotate, while centrifugal force and back pressure make the blade heads tightly adhere to the inner wall of the cylinder, and drive the blades to reciprocate along the blade grooves. The rigid body dynamics model of the blades is shown in Fig. 3. The parameters in the model are shown in Table 1.

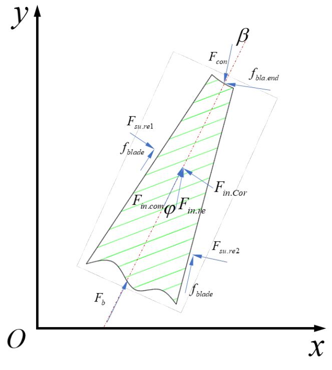

Fig. 3. Schematic diagram of blade rigid body dynamics model

Table 1. List of parameters for the force model of blade rigid body mechanics

Parameter symbols	Parameter meaning
$F_{in.re}$	Convected inertial force
$F_{in.com}$	Relative inertial force
$F_{in.Cor}$	Coriolis inertial force
$F_{su.re}$	Supporting reaction force on both sides of the blade
F_{con}	The force between the blade and the end of the inner wall
f_{blade}	Friction force on the side of the blade
$f_{bla.end}$	Friction force at the end of the blade
F_b	Back pressure chamber pressure, $F_b = (0.7–0.8)P_{ex}$
P_{ex}	Gas discharge pressure
L_{axle}	Rotor shaft length
r_{rotor}	Rotor radius
φ	Rotation angle of rotor
ω	Rotor angular velocity
e	Offset distance
m	Leaf quality
b	Leaf thickness
S	Displacement of blades along the blade groove direction
h	Height of rotor shaft
r	Angle of circular arc sealing section

The distance from the center of mass of the blade to the center of the rotor is expressed as:

$$L_{bl.ro} = \sqrt{\left[r_{rotor} + \left(L_{axle} - r_{rotor}\right)\sin^2\beta\right]^2 + L^2_{axle}/4 - L_{axle}\left[r_{rotor} + \left(L_{axle} - r_{rotor}\right)\sin^2\beta\right]\cos\beta} \quad (2)$$

In the formula, β represents the angle between the contact point of the blade and the inner wall in the opposite and tangential directions.

$$\beta = \arcsin\frac{e}{r_{rotor} + \left(L_{axle} - r_{rotor}\right)\sin^2\varphi} \quad (3)$$

The relative velocity of the blades is:

$$v_r = \omega\frac{d\left(\sqrt{\left[r_{rotor} + \left(L_{axle} - r_{rotor}\right)\sin^2\varphi\right]^2 - e^2} - \sqrt{r^2_{rotor} - e^2}\right)}{d\varphi} \quad (4)$$

The inertial force is expressed as:

$$F_{in.re} = m\omega^2 L_{bl.ro} \quad (5)$$

The relative inertial force is expressed as:

$$F_{in.com} = -m\omega^2\frac{d^2\left(\sqrt{\left[r_{rotor} + \left(L_{axle} - r_{rotor}\right)\sin^2\varphi\right]^2 - e^2} - \sqrt{r^2_{rotor} - e^2}\right)}{d\beta^2} \quad (6)$$

Coriolis inertial force is expressed as:

$$F_{in.Cor} = 2m\omega v_r = 2m\omega^2 \frac{d\left(\sqrt{\left[r_{rotor} + \left(L_{axle} - r_{rotor}\right)\sin^2\varphi\right]^2 - e^2} - \sqrt{r_{rotor}^2 - e^2}\right)}{d\varphi} \quad \textbf{(7)}$$

Friction is expressed as:

$$f_{blade1} = \mu F_{su.re1} \quad \textbf{(8)}$$

$$f_{blade2} = \mu F_{su.re2} \quad \textbf{(9)}$$

$$f_{bla.end} = \mu_m F_{con} \quad \textbf{(10)}$$

In the formula, μ represents the friction coefficient at the contact position between the blade and the rotor, and μ_m represents the friction coefficient at the contact position between the blade and the inner wall of the cylinder. The two friction coefficients are determined by factors such as the material of the contact parts, the roughness of the parts, and the lubrication method. For the convenience of modeling and solving, it is assumed that the friction coefficient remains constant during the operation of the compressor. In the model, it is assumed that there is no deformation of the blades and only rigid body motion occurs, and the following assumptions are made:

1) Neglecting the gravity effect of the blade itself;

2) Neglecting the gas loss during the intake and exhaust processes, that is, assuming that the intake and exhaust processes are in a constant state;

3) Without considering the force of lubricant on the blades and ignoring its impact on the friction coefficient, it is assumed that the friction coefficient is constant;

4) Without considering the impact of fluid chamber leakage on gas pressure, it is assumed that each fluid forms a completely enclosed volume chamber.

The rigid body dynamics model of the blade is represented as:

$$\begin{cases} sign\left(v_r\right) f_{blade1} + sign\left(v_r\right) f_{blade2} + F_{ex} + F_{in.com} - f_{bla.end}\sin\beta = 0 \\ F_{su.re1} - F_{su.re2} + F_{in.Cor} + F_{gas} + F_{con}\sin\beta - F_e \sin\varphi = 0 \\ sign\left(v_r\right)\left(f_{blade2} - f_{blade1}\right) b/2 + F_{su.re1} \cdot L_{bl.ro} - F_{su.re1} \cdot S = 0 \end{cases} \quad \textbf{(11)}$$

$$\mathrm{si}\,gn\left(v_r\right) = \begin{cases} 1 & v_r > 0 \\ 0 & v_r = 0 \\ -1 & v_r < 0 \end{cases} \quad \textbf{(12)}$$

In the formula, the angle between the direction of inertia force and the direction of blade motion is associated with blade φ .

3.3 Modeling of Vibration Transmission Path

There are multiple vibration sources in turbine compressors, and the transmission of mechanical vibration can be compared to a network composed of interconnected nodes. There is a specific path of interconnection between nodes, and the information transmitted between two nodes is vibration or noise. Due to the coincidence of vibrations, the collected vibrations are a mixture of multiple vibration sources. In this section, the vibration separation method is used to search for the main vibration transmission path [14].

In the compressor, the contact points and vibration points between the fluid and the body are regarded as excitations, and the generated vibrations are regarded as outputs, establishing a transfer matrix. Let B be the output of the target point, A_i is the input of the incentive point, and C_i is the transfer function between the target point and the i -th incentive point. Therefore, the mechanism of vibration transmission path is expressed as follows:

$$B=\begin{bmatrix} A_1 & A_2 & \cdots & A_n \end{bmatrix}\begin{bmatrix} C_1 \\ C_2 \\ \vdots \\ C_n \end{bmatrix} \tag{13}$$

The process of obtaining the transfer function is to apply force hammer excitation or exciter excitation at the input end, and then collect the force signal at the input end and the vibration signal or sound signal at the output end, and then estimate and calculate the transfer function. Assuming there are t vibration target points, the corresponding representation method for the target points is as follows:

$$\begin{bmatrix} X_1 \\ X_2 \\ \vdots \\ X_t \end{bmatrix}=\begin{bmatrix} C_{11} & C_{12} & \cdots & C_{1N} \\ C_{21} & C_{22} & \cdots & C_{2N} \\ \vdots & \vdots & \vdots & \vdots \\ C_{t1} & C_{T2} & \cdots & C_{tN} \end{bmatrix}\begin{bmatrix} J_1 \\ J_2 \\ \vdots \\ J_N \end{bmatrix} \tag{14}$$

$$\begin{bmatrix} J_1 \\ J_2 \\ \vdots \\ J_N \end{bmatrix}=T_{ij}^{-1}\begin{bmatrix} H_1 \\ H_2 \\ \vdots \\ H_m \end{bmatrix} \tag{15}$$

In the formula, X_t is the response of the t -th target point, C_{tj} is the transfer function between the t -th target point and the j -th excitation source, and J_j is the j -th excitation source. By substituting the corresponding reference point, the following formula is obtained:

$$\begin{bmatrix} X_1 \\ X_2 \\ \vdots \\ X_t \end{bmatrix}=\begin{bmatrix} C_{11} & C_{12} & \cdots & C_{1N} \\ C_{21} & C_{22} & \cdots & C_{2N} \\ \vdots & \vdots & \vdots & \vdots \\ C_{t1} & C_{T2} & \cdots & C_{tN} \end{bmatrix} T_{ij}^{-1}\begin{bmatrix} H_1 \\ H_2 \\ \vdots \\ H_m \end{bmatrix} \tag{16}$$

T_{ij} represents the transfer function between incentive point i and reference point j . When vibration occurs, different vibration sources need to be separated, and the separation process is illustrated in Fig. 4.

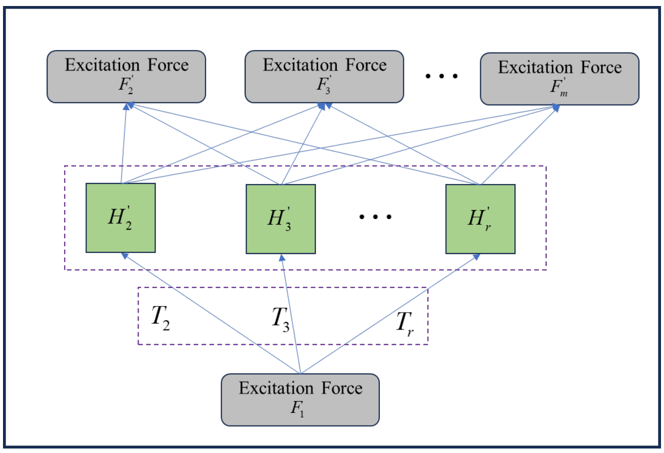

Fig. 4. Schematic diagram of vibration separation process

Assuming that vibration source 2−*r* has *r*−1 reference points H_2, H_3, …, H_r, the net response caused by vibration source 2−*r* is expressed as:

$$\begin{bmatrix} H_2^{'} \\ H_3^{'} \\ \vdots \\ H_r^{'} \end{bmatrix} = \begin{bmatrix} H_2 \\ H_3 \\ \vdots \\ H_r \end{bmatrix} - C_1 * \begin{bmatrix} T_2 \\ T_3 \\ \vdots \\ T_r \end{bmatrix} \tag{17}$$

In the formula, T_i is the transfer function. After calculating the static response, the interface load force at excitation point 2−*r* is calculated using the inverse matrix method. The excitation force of the vibration source is represented as:

$$\begin{bmatrix} F_2^{'} & F_3^{'} & \cdots & F_m^{'} \end{bmatrix} = \begin{bmatrix} H_2^{'} & H_3^{'} & \cdots & H_r^{'} \end{bmatrix} T_{ij}^{-1} \tag{18}$$

When calculating the excitation force of the vibration source on the overlapping path, the excitation force can be calculated first, then the transfer matrix can be multiplied by the vibration source, and finally the difference can be made to obtain the actual excitation force [15]. The calculation principle diagram is shown in Fig. 5.

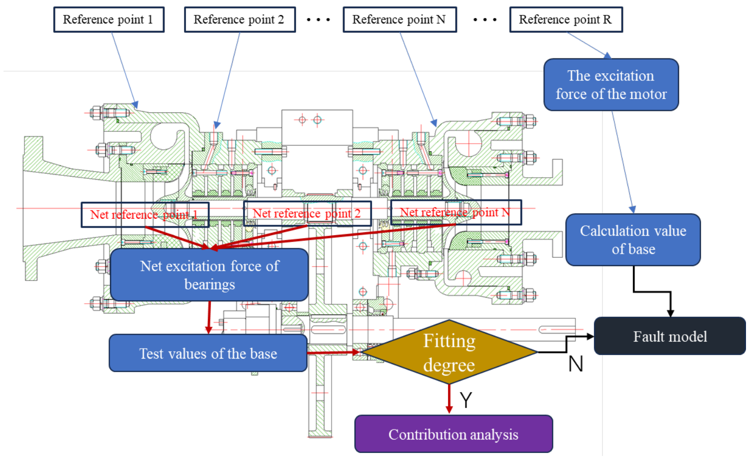

Fig. 5. Principle diagram of incentive transmission

After calculating the actual excitation of each vibration source, calculate the response B of the target point.

$$B = \begin{bmatrix} F_1 & F_2^{'} & \cdots & F_m^{'} \end{bmatrix} \begin{bmatrix} C_1 \\ C_2 \\ \vdots \\ C_m \end{bmatrix} - F_1 * \begin{bmatrix} CH_2 \\ CH_3 \\ \vdots \\ CH_r \end{bmatrix} T_{ij}^{-1} \tag{19}$$

The fitting degree between the calculated and tested values of the target point obtained through this decoupling method in this section is significantly better than that of the classical transmission path algorithm. This method calculates the net response of the overlapping path reference point, and then uses the inverse matrix method to calculate the excitation force of each path, improving the accuracy of load identification and calculating the contribution of the transmission path. Further analysis of the noise path, study of the sound radiation characteristics of the compressor casing, and construction of a sound analysis model provide a theoretical basis for further noise optimization.

4 Vibration and Noise Optimization

Through the analysis in the third section, the model of the vibration source and the corresponding model of the vibration propagation path have been determined. Based on the above two models, by collecting and separating sound, the generation of vibration can be reduced, and improving the vibration transmission path can effectively reduce the vibration noise of the turbine compressor. By studying the sound radiation characteristics of the compressor casing, it is helpful to reduce the noise level of the compressor, construct sound radiation characteristics and modal analysis characteristics, optimize the turbine compressor casing, determine the reasonable distribution position of reinforcement ribs and rib plates, thereby reducing the vibration of the casing and reducing radiation noise [16]. Building a sound analysis model:

$$P_{voice} = \frac{1}{v_c^2}\frac{\partial^2 \Delta P_{voice}}{\partial t^2} \tag{20}$$

In the formula, P_{voice} represents sound pressure, v_c is sound velocity, and Δ is the Prass operator. The Helmholtz equation is used to calculate the sound radiation problem, and the identifier method is as follows:

$$\Delta^2 p + k^2 p = 0 \tag{21}$$

k is the number of sound waves, and using Green's formula and weighted residual method, the Helmholtz equation of the sound field can be derived [17]:

$$C(p)P_{voice}(p) = \int_s \left[izkv_n(Q)G(p,Q)\right]dS \tag{22}$$

In the formula, v_n is the normal velocity of sound particles on the boundary surface S, p is a certain field point in space, P_{voice} is the sound pressure, z is the impedance characteristics of the sound field, where $z = pc$, p are the medium density, v_c is the sound velocity, Q is a point on the boundary surface, $G(p,Q)$ is the fundamental solution of the Green's function, $C(p)$ is a constant that determines the position of point p in the sound field, expressed as follows:

$$C(p) = \begin{cases} 0 & \text{Within the boundary} \\ 0.6 & \text{on the boundary} \\ 1 & \text{Beyond the boundary} \end{cases} \tag{23}$$

The advantage of acoustic boundary element method in numerical solution is that it can reduce the dimensionality of the problem being processed, reducing the three-dimensional problem to a two-dimensional problem and greatly reducing the number of equations. In the traditional boundary element method, a full coefficient matrix is formed during the calculation process, which limits its application in dealing with high-frequency acoustics and large-scale acoustic field problems. Based on the data on the boundary mesh, the calculation is carried out by applying the normal vibration velocity of the nodes obtained from the vibration response calculation to the boundary element mesh. Firstly, the compressor shell model is subjected to acoustic pre-processing, and the large holes on the shell surface are filled to form a dense outer interface. The surface enveloping method is a commonly used technique in engineering design, primarily for creating complex surface shapes. The basic principle is to move around a central path through a series of curves or surfaces, forming an envelope surface that is the desired surface shape. The envelope method can generate various complex surface shapes, suitable for irregular or special design requirements. By precisely controlling the envelope path and cross-section, high-precision surfaces can be obtained, suitable for various application scenarios such as mechanical parts, automotive bodies, aerospace components, etc. Once the initial parameter settings are incorrect, the adjustment process is cumbersome and requires re calculation and optimization. This article uses the surface envelope method to establish an acoustic boundary element model, and the mesh model is shown in Fig. 6.

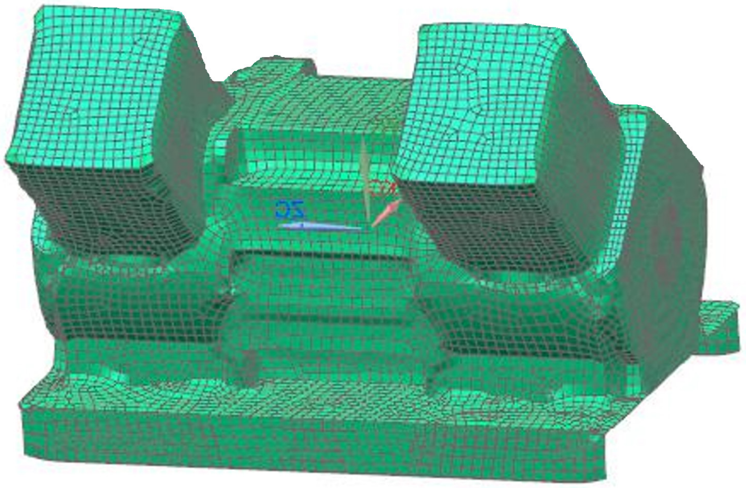

Fig. 6. Acoustic boundary network model

After establishing the acoustic boundary element model, adjust the solver to acoustic properties and define the mesh material as air. Establish a hemispherical surface with a radius of 1m centered on the center of the air compressor base plate, and set it as a microphone grid for acoustic field point calculation. Add a rigid plate on the bottom of the air compressor to simulate the reflection of ground sound waves. The. rst file generated after transient analysis in ANSYS Workbench was imported into the multifunctional simulation platform Simcenter 3D. Due to the fact that the mesh used in transient dynamics analysis cannot be directly used for acoustic calculations, this paper adopts an indirect acoustic calculation method to transfer the vibration velocity of the grid nodes in dynamic response analysis to the acoustic grid nodes and perform Fourier transform processing, thus completing the load transfer processing. Change the solver to acoustic boundary element calculation, use indirect acoustic method, set the disturbance frequency to linear search, range from 12.5*Hz* to 2000*Hz*, and search step size to 12.5*Hz*. The analysis results of the surface sound pressure of the compressor are shown in Fig. 7.

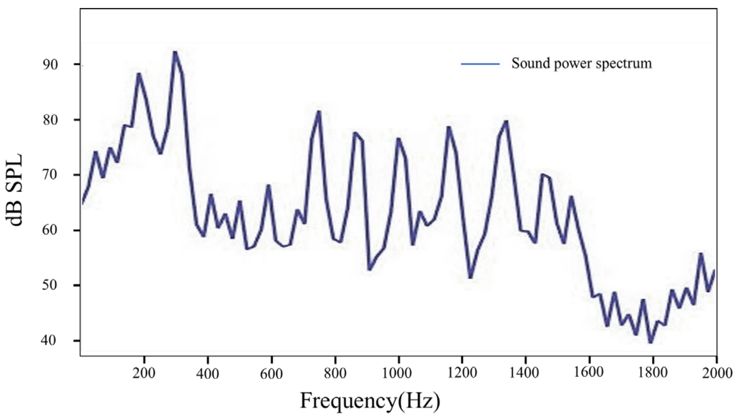

Fig. 7. Surface sound pressure power spectrum response curve of compressor

According to the sound pressure distribution of radiated noise from the body, as the frequency increases, the external sound pressure radiated by the shell changes differently, and the sound pressure level also fluctuates. The specific rules are as follows:

(1) It is found that the shell mainly radiates noise from both sides to one side, indicating that the internal excitation with the same frequency but different phases will result in a frequency difference in the noise radiated outward by the body.

(2) The peak sound pressure level of the radiated noise from the body is at 198 *Hz*, and the sound pressure is mainly concentrated at the top of the scene, indicating that the radiated noise from the four cylinder bodies of this model of air compressor is the highest and exhibits low frequency.

(3) When the frequency is above 450*Hz*, the radiation noise of the air compressor body presents a more complex distribution, with high sound pressure in all four directions and diagonally above, indicating that medium and high frequency noise is generated under various internal excitations. The surface radiated sound power exhibits significant peaks at 130*Hz* -250*Hz* and 370*Hz* -850*Hz*, with the highest reaching 92.6*dB*; After 900*Hz*, the sound pressure level significantly decreases, indicating that the radiated noise from the shell is mainly concentrated in the mid to low frequencies. Comparing the modal natural frequencies of the body, the peak sound pressure at 140*Hz* corresponds to the first-order natural frequency of 145*Hz*, the peak sound pressure at 225*Hz* corresponds to the third-order natural frequency of 237*Hz*, and the peak sound pressure in the frequency range of 370*Hz* to 850*Hz* corresponds to the corresponding modal frequencies, indicating a significant coherence between the radiated noise frequency and the modal frequency.

Based on the above analysis results, this article conducts structural optimization on the compressor housing. For the peak point of radiated noise at 370*Hz* to 850*Hz*, the modal vibration modes are mainly fourth-order and later orders, mainly focused on the internal and external deformation of the side plate and the longitudinal reciprocating bending of the bottom plate side. Therefore, further strengthening of the structural stiffness of the side plate is needed. For the peak point of radiated noise at 150*Hz*, the corresponding first-order modal shape is the cylinder body swinging back and forth, so further strengthening of the structural stiffness is needed. The cylinder body of this model of turbo compressor is made of lightweight aluminum alloy material. The upper and lower cylinder bodies are connected to the body through four bolts, and the lower cylinder body is made transparent in the three-dimensional model. Although this design method facilitates the disassembly process of the cylinder body, it can cause significant structural vibration, and the strength of the bolts directly affects the vibration of the cylinder body. For the peak point of radiation noise at 213*Hz*, the corresponding second-order and third-order modal shapes are lateral overturning of the cylinder body and downward bending on both sides of the body, respectively. Therefore, further strengthening of the structural stiffness is needed. Structurally, the air compressor body is directly connected to the base plate, and the force transmitted from the inside of the body will directly act on the base plate. Therefore, it is particularly important to optimize the design of the base plate structure. According to the modal shape, there is significant longitudinal reciprocating deformation in the bottom plate structure, and its structure is unstable. On the basis of the original model, this article added two reinforcing ribs in the horizontal and vertical directions of the bottom plate. In terms of design, the purpose of supporting the side plate is to further reduce the vibration level of the body by connecting it with the bottom plate and the body. However, due to the small thickness of the side plate itself, it is difficult to withstand the vibration force transmitted from the body. This article increases the structural stiffness by setting reinforcing ribs on the side panels, as shown in Fig. 8. The width and thickness of the reinforcing ribs are both 2mm.

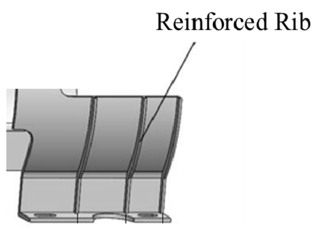

Fig. 8. Schematic diagram of reinforced rib structure design

Through the above process, this article uses acoustic boundary element method to study the acoustic radiation characteristics of the compressor housing, construct the acoustic radiation characteristics and modal analysis characteristics, optimize the turbine compressor housing, determine the reasonable distribution positions of reinforcement ribs and rib plates, thereby reducing housing vibration and radiation noise.

5 Optimize Simulation Results and Analysis

Perform modal analysis, transient dynamics simulation, and acoustic radiation simulation on the optimized model with the same boundary conditions, and compare the optimization effect of surface acoustic radiation noise reduction through the results of pre - and post simulation. Modal analysis mainly studies the dynamic characteristics of structures, which are related to the material properties and geometric parameters of the structure. By constraining the modes, the natural frequencies and corresponding vibration modes of the structure under specific conditions can be obtained. These parameters are of great significance for analyzing the vibration characteristics of the structure and even optimizing the structure. Modal analysis adopts the same grid partitioning method as transient dynamics analysis, with a default element size of 10mm, under which the model grid distribution is uniform. The vibration response before and after optimization is shown in Table 2. Select response vibration node B as the experimental object.

Table 2. Comparison of root mean square velocity of optimized nodes

	Node	A	B	C
Root mean square of vibration velocity in all directions(*mm*/*s*)	V_x	11.96	10.38	9.29
	V_y	12.84	10.92	12.36
	V_z	7.56	8.03	9.38

The calculated vibration intensity of the compressor is 9.78 mm/s, which is 39.7% lower than the original model vibration intensity. The optimized compressor meets the national standard for vibration intensity of V-shaped compressors. Compressor vibration intensity refers to the vibration intensity generated by mechanical equipment during operation, usually represented by the maximum, average, or root mean square value of parameters that characterize the vibration level (such as displacement, velocity, and acceleration). The International Organization for Standardization (ISO) recommends using the root mean square value of vibration velocity to represent vibration intensity, as it contains frequency information, reflects the energy of the vibration system, and takes into account the time history of the vibration process [18]. The optimized vibration time domain and frequency spectrum of the body shell are shown in Fig. 9.

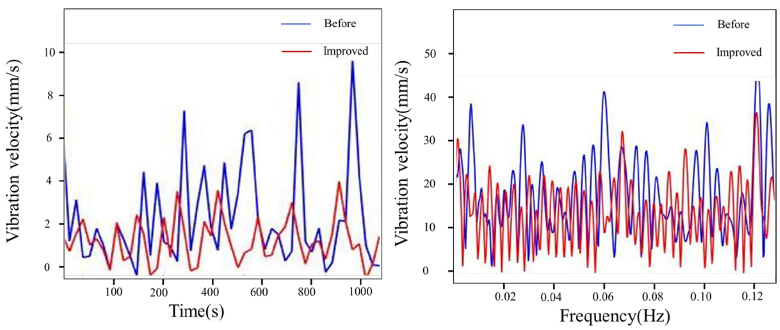

Fig. 9. Comparison of time domain and frequency domain vibration velocity of node B

Based on the acoustic boundary model in Chapter 4, surface acoustic radiation calculations were performed and surface acoustic power was compared. The comparison results are shown in Fig. 10.

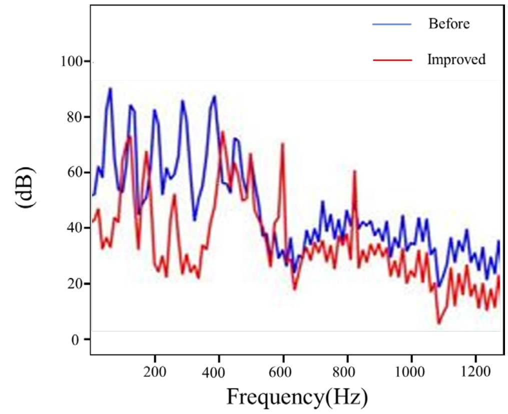

Fig. 10. Comparison curve of sound radiation power frequency response

Through comparative analysis, the overall radiated sound power of the optimized model shows a decreasing trend, and the frequency of the corresponding peak point has also increased. According to acoustic software measurements, the total sound power of the signal decreased from 88.2dB to 81.6dB, with a decrease of 6.6 dB.

This chapter mainly introduces the simulation optimization results of the compressor. Through optimization analysis, the vibration and noise of the compressor after structural optimization can be reduced by 39.7%, which is in line with the expected effect.

This section establishes a three-dimensional model of the air compressor casing, and studies the vibration response characteristics of the casing by applying main bearing forces and relevant constraints [19]. The vibration intensity of the air compressor casing and the vibration time-domain data and frequency spectrum of each node of the cylinder body are calculated. Then, a constrained modal analysis was conducted on the casing, obtaining the first ten natural frequencies and vibration modes, and preliminarily evaluating the vibration form and weak links of the casing. Subsequently, an acoustic boundary element model of the air compressor housing was established using Simcenter 3D [20]. The surface normal vibration velocity was used as the input condition, and the indirect acoustic method was used to calculate the sound pressure distribution of the external radiation field of the air compressor housing. The conclusion was drawn that the cylinder body is the main component of the air compressor's external radiation noise and the main frequency range of the body's radiation noise. Then, based on the constrained modal results, reinforcement ribs were installed on the bottom and side plates of the air compressor, and the diameter of the cylinder support bolts was increased to improve the stiffness of the weak structural components of the air compressor. Simulation results of the optimized model showed that the natural frequencies of the casing were significantly increased, and the near-field radiated noise power was reduced, achieving the goal of noise reduction.

6 Conclusion

This article establishes a mathematical analysis model for mechanical excitation of rotary vane compressors and fluid excitation by internal flow field airflow pulsation

The dynamic model, whole machine vibration response dynamic model, and acoustic boundary element model were used to clarify the mechanical excitation and airflow pulsation excitation mechanisms of the compressor. The vibration response characteristics of the compressor were analyzed, and the propagation mechanism and distribution law of radiation noise were revealed based on the prediction model. Noise testing research was conducted to verify the rationality of the prediction model. The main conclusions drawn are as follows:

1) In depth analysis of turbine compressors has been conducted, and the vibration mechanism and transmission path of turbine compressors have been analyzed and modeled. The model serves as a basis for further analysis, and the establishment of the model requires more accuracy and higher precision.

2) Completed the analysis of the sound radiation characteristics of the compressor housing, constructed the sound radiation characteristics and modal analysis model, optimized the turbine compressor housing, determined the reasonable distribution position of the reinforcement ribs and rib plates, and constructed the sound analysis

model. The reinforcement ribs were used as optimization means, and the optimized model effect needs to be analyzed.

3) Perform modal analysis, transient dynamics simulation, and acoustic radiation simulation on the optimized model with the same boundary conditions, and compare the optimization effect of surface acoustic radiation noise reduction through the results of pre - and post simulation.

There are some shortcomings in the research content of this article, but given the complexity of studying air compressor noise and the constraints of research time and related research conditions, there are still certain issues that deserve further in-depth exploration in the future:

1) This article mainly uses simulation verification to optimize the structure of air compressors, lacking experimental support

Support, in the future, trial production of engineering prototypes can be carried out to verify their effectiveness through experimental methods.

2) Due to the fluctuation of gas pressure inside the air compressor, the noise at its inlet and outlet is also noise

A significant source that can be further studied for intake and exhaust noise.

3) This article uses acoustic boundary element method to predict the radiated noise of air compressor casing and establishes a scene

There are certain limitations to inferring the noise radiated by specific structures based on the near field of the hemisphere. Future can be built

Surface acoustic field of air compressor, and then directly study the radiation noise characteristics of air compressor structure.

7 Acknowledgement

This work was supported by the Tianjin Research Innovation Project for Postgraduate Students [2023KJ259].

References

[1] J. Zhang, G.-Y. Liang, L.-P. Qi, Application of Multi-dimensional Intelligent Control Technology for Large Scale Turbine Compressor, Automation in Petro-Chemical Industry 60(2)(2024) 30-34.

[2] G.-F. Ma, W. Zhang, M.-Y. Zeng, Cause Analysis on Scaling of Compressor Turbine in Ethylene Plant and Solutions, Petrochemical Equipment Technology 44(5)(2023) 54-61+66+7.

[3] Y.-L. Li, G.-Q. Zhong, E.-L. Wu, Y. Yang, Analysis of the Causes of High Vibration in Gas Turbine Compressors, Chemical Equipment Technology 44(3)(2023) 64-67.

[4] W.-Z. Zhang, Z. Qu, B.-Q. Li, X.-M. Xu, Z. Wang, J.-G. Chen, W.-G. Yan, H.-K. Li, Research on noise characteristics and suppression methods of variable frequency scroll compressor, Fluid Machinery 51(11)(2023) 79-85.

[5] H. Liu, C.-Y. Chen, Research on a Fault Detection Technology for Non-contact Compressor Operation, Industrial Control Computer 35(8)(2022) 5-6+9.

[6] S.-X. Luo, Z.-Y. He, P.-A. Tao, H.-M. Liu, L.-Z. Hu, S.-Z. Sun, Prediction and tests for vibration and noise of exhaust valve plate of rotary vane compressor based on fluid-structure interaction, Journal of Vibration and Shock 41(19)(2022) 266-273.

[7] B.-X. Long, J.-M. Chen, Z.-H. Chen, Z.-Z. Liu, D.-X. Liao, Aero-acoustic performance of a continuous transonic wind-tunnel axial-flow compressor, Journal of Northwestern Polytechnical University 40(4)(2022) 829-836.

[8] Y.-Z. Li, Q. Wu, Y. Lv, L.-L. Tan, C.-J. Yi, Noise Test Analysis and Control of Centrifugal Compressor, Journal of Qingdao University (Engineering & Technology Edition) 36(4)(2021) 67-72.

[9] Z.-F. Luo, H.-L. Li, J.-J. Li, F. He, Noise simulation and test of small two-cylinder reciprocating compressor, Journal of Chongqing University of Technology (Natural Science) 38(3)(2024) 260-266.

[10] W.-N. Jin, F.-A. Lu, C.-S. Liu, J.-Q. Ren, H.-L. Wang, H. Yu, Design and Experimental Verification of a Double-layer Perforated Plate Noise Reduction Scheme for a Multi-stage Axial Compressor, Chinese Journal of Turbomachinery 65(5)(2023) 41-44+80.

[11] J.-H. Na, L. Song, P.-S. Hou, Research and Development of Bearing Pedestal of Megawatt Steam Turbine, Foundry Equipment & Technology (3)(2020) 8-10.

[12] Y. Yang, H.-H. Zheng, B.-R. Zhou, Design and application of pipeline vibration reduction for parallel system of rotor compressor, Fluid Machinery 50(10)(2022) 76-82.

[13] Y.-G. Zhang, J.-X. Hu, H.-P. Liu, A.-H. Dong, Prediction of Mechanical Performance of Turbine Blade based on Sequential Stochastic Kriging Model, Turbine Technology 64(4)(2022) 241-245+266.

[14] G. Chen, Vibration and Sound Radiation Mechanism and Transmission Path of Steam Turbines Based on Multibody Dynamics, China Offshore Platform 39(3)(2024) 60-67.
[15] X.-F. Chen, J. Li, R. Guo, Response Analysis for a Vertical Vibration Model of Four-roller Cold Rolling Mill under Gaussian Colored Noise Excitation, Journal of Hainan Normal University (Natural Science) 36(4)(2023) 387-392.
[16] X.-D. Sun, Y.-F. Zhang, S.-B. Zhao, H.-J. Shi, Simulation analysis and optimization design of aerodynamic noise in the cylinder head of refrigeration compressor, Journal of Appliance Science & Technology (S1)(2023) 242-246.
[17] W.-W. Wu, W.-C. Pan, P.-Y. Zhao, Numerical analysis of relative low frequency noise transmission loss of Helmholtz resonators under a Grazing flow, Ship Science and Technology 44(7)(2022) 62-67.
[18] B.-Y. Ma, Z.-S. Lian, H.-C. Mao, Fault feature extraction of valve spring of emulsion pump based on vibration intensity, Machine Tool & Hydraulics 52(7)(2024) 201-207.
[19] Y.-J. Luo, K.-P. Wu, Y.-M. Rao, T.-K. Wu, Study on Vibration Performance of Cylinder Structure of Internal Combustion Engine Under Piston Knocking Force, Internal Combustion Engine & Parts (6)(2024) 51-53.
[20] X.-F. Zhang, Y. Shao, Y.-Q. Fu, L. Quan, Mechanical and Hydraulic Co-simulation Analysis for Crane Luffing System based on Simcenter 3D, Journal of Mechanical Engineering 58(24)(2022) 334-341.